Title

EXPLORATORY STUDY OF SOOT SAMPLE INTEGRITY AND PROBE PERTURBATION IN A SWIRL-STABILIZED COMBUSTOR.

Journal

Journal of engineering for power, 103(4)

ISSN

0022-0825

Authors

Hack, RL
Samuelsen, GS
Poon, CC
et al.

Publication Date

1981

DOI

10.1115/1.3230799

R. L. Hack
Research Assistant.

G. S. Samuelsen
Associate Professor.
Mem. ASME

Mechanical Engineering,
University of California,
Irvine, Calif.

C. C. Poon
Staff Scientist.

W. D. Bachalo
Senior Scientist.
Mem. ASME

Spectron Development Laboratories,
Costa Mesa, Calif.

An Exploratory Study of Soot Sample Integrity and Probe Perturbation in a Swirl-Stabilized Combustor

In-flame measurements of soot particulate using conventional extractive and nonintrusive optical probes are compared for a swirl-stabilized combustor. Except for large ($\sim 5\mu m$) particulate present in the extracted samples, the soot particle size compares favorably with optically measured values, and the soot particle morphology reflects that formed in gas turbine combustors. Two, nonflame sources for the large particulate are suggested by the optical data: particles formed or elongated during transport subsequent to extraction, and particles attrited from upstream carbon deposits on a solid surface. The extractive probe produces a change in the local particle number density which varies from little change to a 70-fold suppression in reacting flow and a 200-fold increase in cold seeded flow depending on the location within the combustor of the optical sampling volume, the location of the extractive probe relative to the optical sampling volume, and the combustor operating conditions.

Introduction

A primary challenge in the operation of gas turbine engines on broad specification and alternative fuels is the propensity of these fuels to form soot. Approaches under consideration to reduce this soot production include combustor modification, and the use of smoke-suppressant fuel additives. The severe economic penalties associated with retrofit make combustor modification more appropriate for new engines whereas the use of smoke-suppressant fuel additives is more appropriate for existing gas turbine engines. Implementation of either control approach first requires the experimental evidence (1) to identify the causal effects of fuel properties, additive properties, and combustor operating conditions on soot formation, and (2) to evaluate and develop models destined for turbine design.

Experimental studies in progress that address the sooting associated with alternative and broad specification fuels are oriented toward the *gross* soot emission and radiation from simple flames (e.g., [1]), well-stirred reactors (e.g., [2]), and production combustors (e.g., [3]). As the interest focuses on the mechanics of soot formation, so does the need to measure *local* properties of soot such as number density, weight concentration, and particle size distribution. Extractive probes have been and continue to be used (e.g., [3,4]) for these measurements. The use of such techniques is dictated by state-of-the-art and cost. The only viable alternatives are nonintrusive, optical methods which are in their infancy in development.

Two major questions are associated with the use of extractive probes:

- *Representativeness of Sample.* Is the extracted sample representative of the particulate at the probe entrance or do the processes of extraction, transport, and subsequent deposition of the particulate on a filter transform the morphology and number density of the soot?

- *Flow Perturbation.* Does the presence of the probe in the flow perturb the local conditions (e.g., temperature, aerodynamics, chemistry) and thereby produce a condition at the probe entrance that is different from that which occurs in the absence of the probe?

These questions are especially important in flows, such as those that occur in gas turbine combustors, where the aerodynamics includes swirl and flow reversal.

This paper presents data on both the representativeness of the sample and probe perturbation in a swirl-stabilized combustor using nonintrusive optical techniques focused at the entrance of an extractive probe. The optical techniques are on the forefront of technology for point measurements in flows dominated by strong aerodynamics. As such, optical sizing in the present case is limited to particles with diameters in excess of $0.3\mu m$. The net result is that the present results are exploratory, and not exhaustive. However, the results reveal the type of problems introduced by extractive probes, specific questions that must be raised in the interpretation of data from extractive and optical probes, and the type of experiments necessary to develop and test soot measurement methods in order to insure that the data obtained are representative of the events that occur within swirl-stabilized combustors.

Contributed by the Gas Turbine Division and presented at the International Gas Turbine Conference, Houston, Texas, March 8-12, 1981, of THE AMERICAN SOCIETY OF MECHANICAL ENGINEERS. Manuscript received at ASME Headquarters, December 5, 1980. Paper No. 81-GT-27.

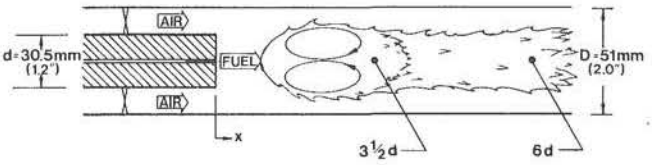

Fig. 1 Combustor configuration

Experiment

Combustor Configuration. The combustor configuration is presented in Fig. 1. The combustor housing is 51mm (2 in.) o.d. quartz tubing. The internal centerbody and annular air jet swirl provide a stabilized recirculating flow concentrated in the center of the combustor. The fuel is introduced through a central jet with a 1.3mm (0.052 in.) diameter. The angle of swirl is 60 deg and the blades are located 57mm (2¼ ins.) upstream of the centerbody face. The principal criteria for the selection of this combustor design were the inclusion of complex (i.e., turbulent, reverse flow) aerodynamics and optical accessibility.

Test Conditions. The test conditions are itemized in Table 1. The range of reference velocities was selected to (1) be representative of those produced in practical combustors, (2) span a range of operating conditions, and (3) bracket effects observed in the probe perturbation studies. The mixture ratios were selected to (1) be representative of those in practical combustors, and (2) in the case of $\phi = 0.37$, produce conditions suitable for good optical measurements. Finally, the sampling locations were selected to represent a point in the wake of the zone of recirculation, and within the zone of recirculation.

The combustor was operated on gaseous ethylene.

Table 1 Test conditions

Reference velocity[1] U_{ref} (m/s)	Overall equivalence ratio[2] ϕ	Sampling location[3] (x/d)
0.65	0.2	6
5.5	0.2, 0.37	6, 3½
7.5	0.2, 0.37	6
15.0	0.2	6

1. cold flow velocity referenced to duct diameter, 51mm (2 in.)
2. actual overall fuel-to-air ratio divided by stoichiometric ratio
3. x,d: Refer to Fig. 1

Extractive Probe. The probe and sample systems used in this study (Fig. 2) are of conventional design. The probe is constructed of stainless steel throughout with a 9.5mm (3/8 in.) outside diameter and a 3.0mm (1/8 in.) i.d. sampling tube. The overall length of the probe is 914mm (36 in.) including a large radius bend in order to clear the combustor exhaust stream. The probe is water cooled to approximately 80°C and has isokinetic pressure ports, a gas sampling port for gas analysis, and an inert gas injection port. The purpose of the latter is to dilute the mixture, quench reactions, and prevent deposition along the walls.

The remainder of the system consists of a heated sample line to prevent condensation leading from the probe to an oven. The oven, heated to 80°C, contains a two stage filter utilizing 47mm Nuclepore membrane filters: 5μm pore size for the primary filter and 0.2μm pore size for the secondary. Nuclepore filters were chosen for their adaptability to scanning electron microscopy (SEM).

Sample analysis proceeded by drying and cooling the filters in an oven and a desiccator, respectively. Sample times were 10 minutes. Size analysis and physical characterization of the particles were conducted utilizing a scanning electron microscope.

The 9.5mm (3/8 in.) probe diameter is the smallest reasonable size to incorporate the necessary ports and provide clearance for sample transport. As a result, the probe to combustor duct diameter is large (3/8 in. to 2 in.). However, this proved beneficial in the present study by enabling the demonstration of blockage. In particular, combustor operating conditions were established for which blockage by the extractive probe dominated the results, and conditions were identified for which blockage did not influence the results.

Optical Probe. Figure 3 provides a schematic diagram of the dual range optical probe. Two techniques, scattering intensity ratioing [5] and particle sizing interferometry [6], are used. For the configuration employed, the scattering intensity ratioing is sensitive to particles in the size range of 0.3 to 1.8μm. The particle sizing interferometry is sensitive to particles in the size range of 2 to 7.5μm.

An argon-ion laser operating in multiline mode serves as the light source for the system. The laser lines are separated with the use of a disperion prism and the two dominant lines, 0.5145μm (green) and 0.4880μm (blue), are directed through separate optical paths.

For scattering intensity ratioing, the blue beam is expanded by a factor of 3.5 to produce the required beam diameter. Because the small particles are typically more numerous and scatter less light, and beam must be focused to the minimum possible diameter which, for the present case, is approximately 50μm.

The beam (green) used for particle sizing interferometry is partitioned into two equal intensity beams with a path-matched beamsplitter. A mirror system is then used to recombine and focus the two beams at a common point in the flow field. Where the green beams cross, an interference fringe pattern of spatially varying light intensity is formed. Superimposed on this is the highly focused blue beam for the scattering intensity ratioing technique.

Light scattered by particles passing through the focused beams is collected by a system of lenses. The scattered light from each of the two wavelengths, 0.5145μm and 0.4880μm, is separated and directed to the appropriate photodetectors. Half of the scattered light is viewed by PMT-3 for interferometric processing. The other half passes through a system of masks which consists of annular ring openings in order to admit the scattered light at only the two scattering angles used. These masks also serve to effectively limit the length of the measurement region. The two photodetectors, PMT-1 and PMT-2, in turn transform these angularly selected rays into electronic signals which are then processed for validation and graphical display.

The interpretation of measurements using these two techniques is based on the analysis of the Mie scattering properties of a homogeneous, isotropic spherical particle. In order to apply these two techniques with confidence, the effects caused by nonspherical scatterers with an uncertain index of refraction require special considerations. For nonspherical scatterers, Hodkinson [7] showed that the forward scatter for a polydisperse system of irregular particles was similar to that of spherical particles of equivalent projected cross-sectional area. Hirleman [5] investigated the scatter from irregularly-shaped particles formed by agglomerated polystyrene spheres and found that the scattering patterns had forward lobes that appeared similar to those of spheres of equivalent diameter. In terms of the intensity ratioing technique, Hirleman also computed the scatter for particles of short aspect ratios and found that the

maximum error due to nonspherical particles was about 40 percent.

The effect due to an uncertain index of refraction was inspected in detail by both Chu and Robinson [8] and Hirleman [5]. Their findings show that, for absorbing particles (as is the case with soot particles), the errror due to an uncertainty in the index of refraction is very small (typically several percent). However, for the nonabsorbing particles, as is the case in the cold flow conditions described below, the error in both techniques can be as much as 25 percent, depending on the actual size of the particles.

Another effect, common to both techniques, which will cause additional error is due to the depth of field. In both techniques, an out-of-focus particle will generally infer a size larger than the sphere of equivalent cross-sectional area from the observed scattered light. Hirleman [5] dealt with this problem and provided solutions. However, in the present situation, out-of-focus particles could not be conveniently optically discriminated using his method. Therefore, the depth of field effect results in a broadening of the size distribution, especially in the large size end. The error in size produced by this effect is less than 30 percent.

In this study, two kinds of sizing conditions were encountered. The first was the cold flow conditions which, as will be seen below, consisted of sizing specified-size particles. Since these particles were nonabsorbing and appeared to be spherical, the combined error according to the above analysis would be 20-30 percent with some broadening of the distribution. The second was the hot flow conditions where soot particles were measured. These particles were expected to be nonspherical but should be absorbing. The combined error would then be 20-30 percent with some broadening of the distribution.

To evaluate the performance of the optical probe, size measurements using specified-size particles were first conducted under cold flow conditions. Two specified-size spherical polystyrene particles were used: 3.3μm (0.12μm SD) and 0.48μm (0.0018μm SD) (Dow Diagnostics, Indianapolis, IN). These two sizes were selected so that each of the two optical sizing techniques could be tested. The test particles were obtained by diluting 300 times the original particle/water mixture using double-filtered (0.2μm filter paper) deionized water. Seeding of these particles was accomplished using a nebulizer located 2m upstream of the centerbody. At this location, it was experimentally determined that pure water droplets produced by the nebulizer would completely evaporate.

To observe the 3.3μm diameter particles, particle sizing interferometry was used. A fringe spacing of 7μm was established thus making the instrument sensitive to particles between 2 to 7.5μm. Measurements were obtained at three axial locations downstream of the centerbody and at a number of flow conditions. Measured mean diameters ranged from 3 to 4μm with a standard deviation near 1μm and a most probable diameter ranging from 2.8 to 3.4μm. Figure 4(a) shows measurements obtained at an axial station 6d downstream of the centerbody (where d is the diameter of the centerbody) resulting in a mean diameter of 3.4μm, a standard deviation of 1.0μm, and a most probable diameter of 3.3μm. The large mean diameter and standard deviation can be accounted for by the broad tail on the large diameter side of the distribution. This tail was determined to be excessively broad for monodispersed particles even though the test

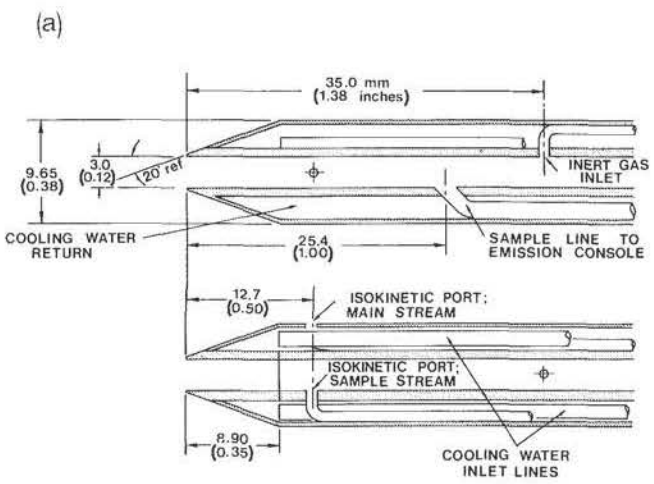

Fig. 2(a) Extractive Probe

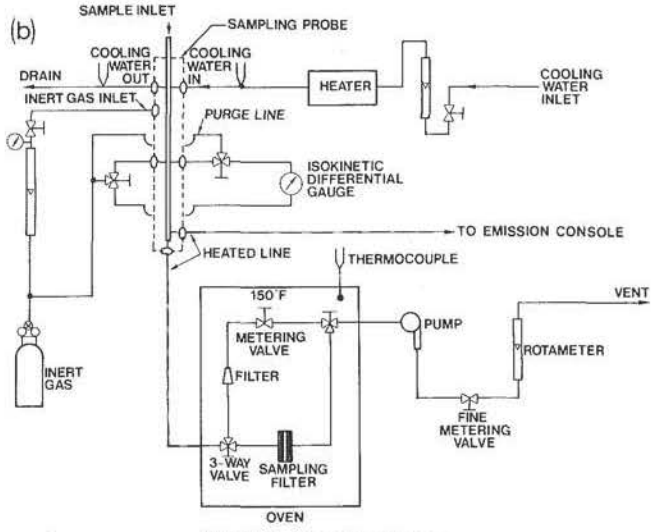

Fig. 2(b) Sampling System

Fig. 2 Extractive probe and sampling system

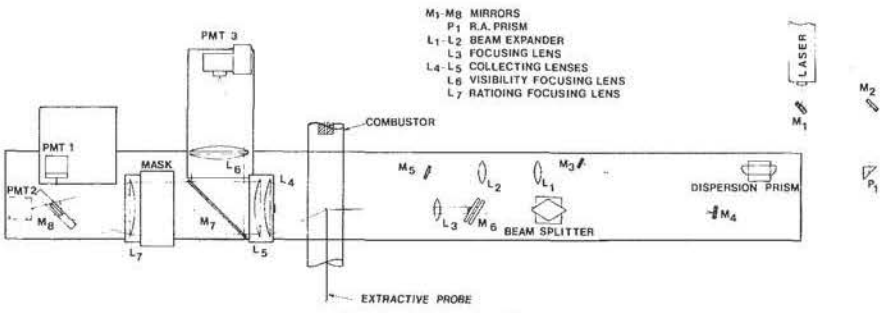

Fig. 3 Optical probe

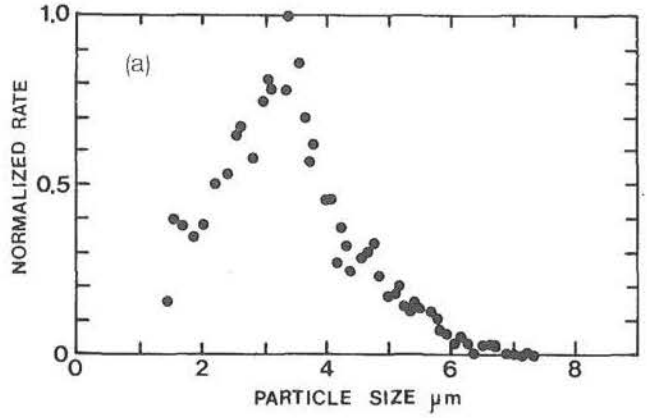

TOTAL RAW COUNT=2136
TOTAL REDUCED COUNT(MM-2)=35543
LINEAR MEAN=3.4
SURFACE MEAN=3.6
VOLUME MEAN=3.7
SAUTER MEAN=4.1
STANDARD DEV= 1

MEAN VELOCITY(M/S)=10.74
RMS VELOCITY(M/S)=1.97

Fig. 4(*a*) Interferometric data (3.3μm particles)

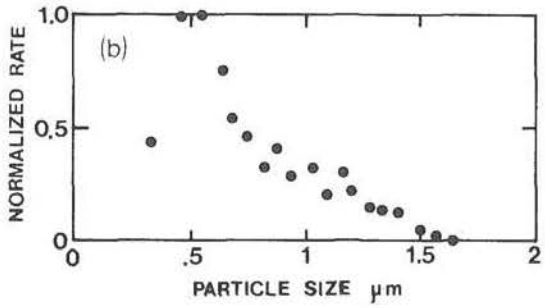

TOTAL RAW COUNT= 1669
TOTAL REDUCED COUNT= 107936.4
LINEAR MEAN = .75
SURFACE MEAN = .81
VOLUME MEAN = .86
SAUTER MEAN = .97
STANDARD DEV = .29

SAMPLE TIME= 180.1

Fig. 4(*b*) Ratioing data (0.48μm particles)

Fig. 4 Optical probe validation – nonreacting flow with seeding (U_{ref} = 7.5mps)

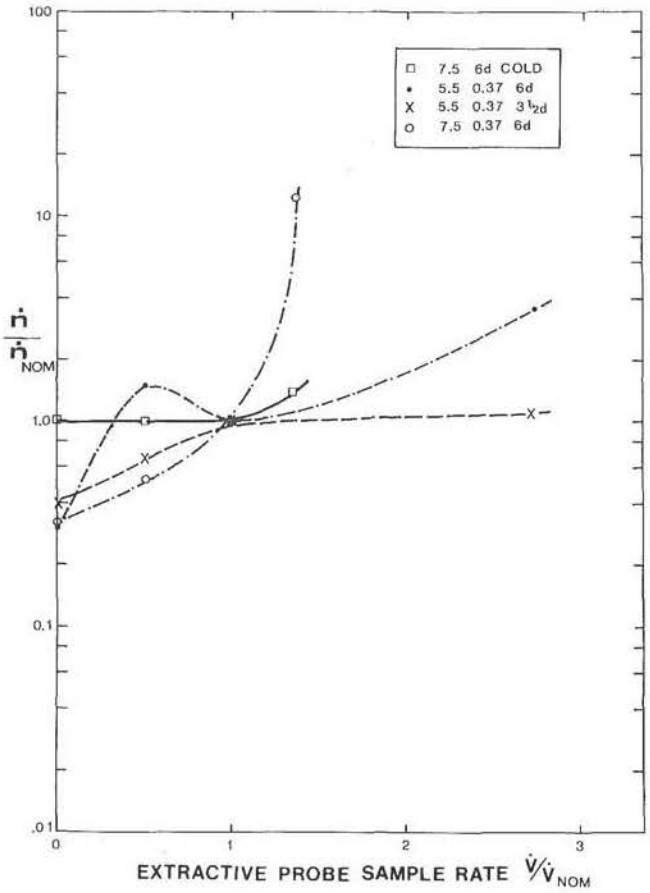

Fig. 5 Extractive probe conditions – effect of sampling flowrate on optically measured data rate

particles were nonabsorbing. Thus the broadening was suspected to be due to effects other than nonspherical particles or an uncertain index of refraction as mentioned before. Probable causes for the broad tail were: finite optical depth of field, particle agglomeration, and the liquid emulsifier (present with the seed particles and with a low vapor pressure) which forms a polydispersed distribution of droplets. Parallel studies of these particles using SEM authenticated the mean size to be 3.3μm with a standard deviation of $\sim$0.2μm.

A similar cold flow study was conducted utilizing 0.48μm diameter particles and the scattering intensity ratioing technique. The two scattering angles selected were 6 and 12 deg, thus making the instrument sensitive to particles between 0.3 and 1.8μm. Figure 4(*b*) shows measurements obtained at an axial station 6d downstream of the centerbody. These measurements were analyzed with the assumption that the most probable diameter of the particles was 0.48μm, thus the study served as a calibration of the instrument. Subsequent SEM studies revealed that these particles had a mean diameter of 0.50μm and a standard deviation of $\lesssim$ 0.05μm. The size distribution measured optically has a broad tail (Fig. 4(*b*)) with a standard deviation of 0.29μm. Again, the finite optical depth of field, particle agglomeration, and the presence of the emulsifier were probably responsible for this effect. Simultaneous sizing measurements employing both techniques during this cold flow condition showed that micron size particles were indeed present, thus providing evidence for the existence of large particles and the occurrence of the broad tail. In soot particle sizing measurements, the size broadening effect would not be significant.

Approach

The approach adopted was to position the optical probe at the entrance of the extractive probe for each of the conditions listed in Table 1. First, the conditions of the extractive probe were varied (Table 2) to change the rate of cooling and dilution experienced by the sample. Simultaneously, optical data were obtained to record the impact on the data rate (i.e., local number density) and particle size distribution within the limits of the optical methods (0.3μm to 7.5μm).

Secondly, the position of the extractive probe was changed relative to the optical probe to assess the perturbation produced by the extractive probe. Beginning at the nominal sampling location, the extractive probe was removed axially in incremental steps while the optical probe remained at the original centerline location. The impact of the probe location on the optical probe measurements was recorded in terms of data rate and particle size distribution. In addition, radial

Table 2 Extractive probe conditions

Reference Velocity, U_{ref}[1] (m/s)	Sample flow rate				N_2 Dilution		
	Nominal[2] (cc/min)	High[3] (cc/min)	< Nominal (cc/min)	Zero (cc/min)	Nominal[4] (cc/min)	< Nominal (cc/min)	Zero (cc/min)
0.65	1700	–[5]	–	–	1200	–	–
5.5	3000	8200	1000	–	530	350	0
7.5	7000	9400	3000	0	2100	950	0
15.0	7300	9400	3100	–	1800	–	0

1. Refer to footnote 1, Table 1
2. Flowrate with isokinetic pressure taps balanced
3. Maximum flowrate that can be achieved
4. Rate established to prevent water condensation for all overall ethylene equivalence ratio of 0.30
5. Runs not conducted

profiles of data rate and particle size distribution were obtained optically with and without the extractive probe in the flame.

The results are presented for the *extractive probe conditions* (Figs. 5-9) and *extractive probe perturbation* (Figs. 10-13), respectively.

Results

A. Extractive Probe Conditions

1. Nonreacting Flow With Seeding. The extractive probe conditions were first tested for the case of nonreacting flow by seeding with 0.48μm polystyrene spheres and recording the effect of sample flow rate on the optically measured data rate at the extractive probe entrance. For a 7.5mps reference velocity, the data rate increased 40 percent at the maximum sample rate (Fig. 5), consistent with theories relating to nonisokinetic effects; namely, the higher flow rate promotes the radial convection of small particles into the sampling volume.

2 Reacting Flow.

Extractive Filter Samples. The extractive probe sampling conditions had a significant impact on soot morphology and number density. As discussed later, the sampling conditions had a relatively small impact on particle size in the range observed optically.

One of two morphologies were observed on the primary (5.0μm pore) filters depending on sample condition: Platelet-like structures (Fig. 6(a)) and tightly-packed puff-like structures (Fig. 6(b)).

The puff-like structures occurred for higher overall sample transport temperatures and lower cooling rates. For example, the puff-like structures occurred on the primary filter when the N_2 dilution was reduced (Fig. 6(b)), when the sample rate was increased, or when the equivalence ratio was increased (Fig. 7). As shown in Fig. 6, this behavior was observed whether the reference velocity was 15mps or 0.65mps.

When small particles were observed, the morphology of the particles on the secondary (0.2μm pore) filter was similar (Fig. 6) to the puff-like structures noted above. In particular, they appeared as 0.5 to 1μm agglomerates of smaller ($\sim$.05μm) spherical particles which is consistent with the morphology and size observed in full-scale combustor studies (e.g., [10,11]). The peak size increased as the mixture ratio was enriched (Fig. 7), and as the sampling location was moved closer to the centerbody (3½d compared to 6d). The number density of particles on the secondary filter also increased sharply as the mixture ratio was enriched (Fig. 7) and as the reference velocity was increased (Fig. 6(a)).

At the enriched conditions (ϕ = 0.37), a hybrid of the puff-like structure was observed on the primary filter with zero nitrogen flow (Fig. 8). The sample morphology was akin to a dried mud flat. This is attributed to water condensation on the filter during sampling and subsequent drying of the filter in a desiccator. The water condensation occurred as a result of the sample temperature dropping below the dew point temperature of the mixture, the latter of which was unusually high because of the high concentration of water associated with the high concentration of fuel along the centerline of the combustor.

The addition of nitrogen as a diluent is one approach that can be employed to lower the dew point. The impact of this is shown on the primary filter in Figure 7(b). The puff-like structure is clearly discernable though evidence of some moisture remains.

Optical Measurements. The extractive probe results raise two questions typical of extractive probe samples (1) Are the large particles ($\sim$5μm) on the primary filter present at the probe entrance, and (2) are the smaller particles observed on the secondary filter present at the probe entrance in the agglomerated size ($\sim$1μm) or in the smaller size cut ($\sim$.05μm) of the individual particles that make up the agglomerates?

Interferometric Measurements (2-7.5μm). The interferometric size measurement verified that large particles were in fact present at the probe entrance at the enriched conditions (ϕ = 0.37). For example, at 7.5mps, the interferometric measurements (Fig. 9(a)) indicate the presence of large particles with a peak size of $\sim$4μm. At this condition, approximately 10 particles per second were observed through the optical probe volume while the SEM picture has approximately 90 particles in the field of view. After adjusting these two values to the same basis, the extractive probe sample had a rate of deposition an order of magnitude higher than the data rate observed optically at the probe entrance. This provides evidence that the 5μm puff-like structures are formed after entering the probe. Further evidence is provided by the optical measurements at ϕ = 0.2 at which no interferometric signals were recorded, yet large puff-like structures (Fig. 6(b)) or platelet-like structures (Fig. 6(a)) were deposited on the primary filter.

The mechanics of the large particle formation in the sampling system is not firmly established. The present explanation holds to the scenario that the mixture at the sampling volume is comprised of soot particulate formed well upstream (and subsequently deposited on the secondary filter) and fuel undergoing pyrolysis. This fuel is cooled upon entry into the extractive probe. Rapid cooling leads to the platelet-like structures. Less rapid cooling promotes the formation of

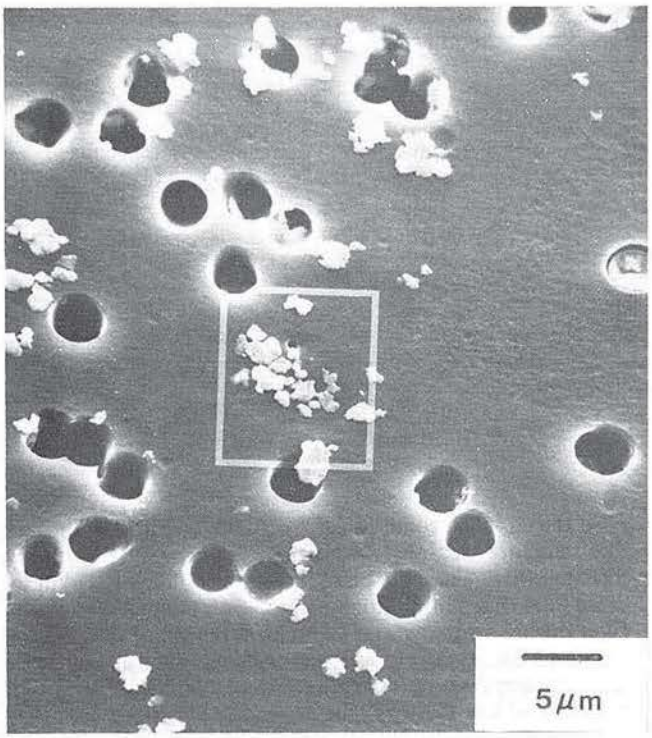

Primary filter – 5μm pore. 0.65 mps

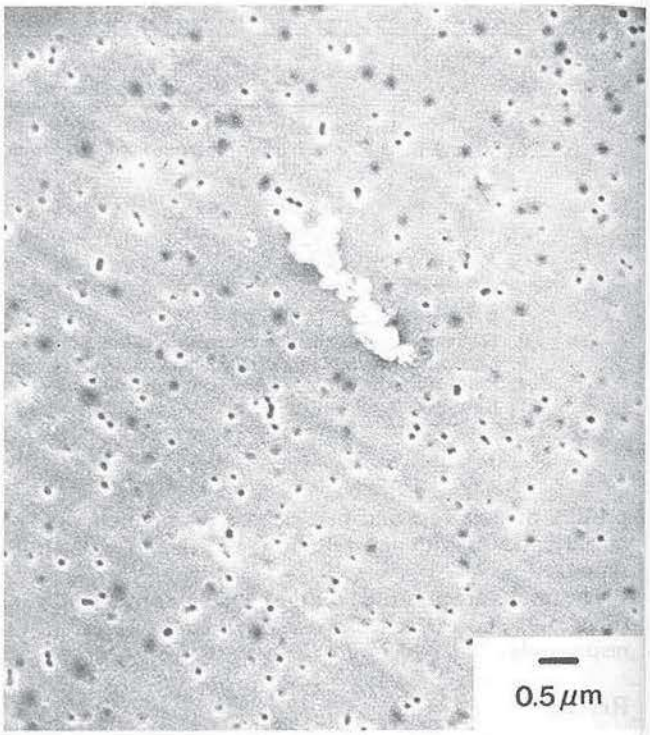

Secondary filter – 0.2μm pore. 0.65 mps

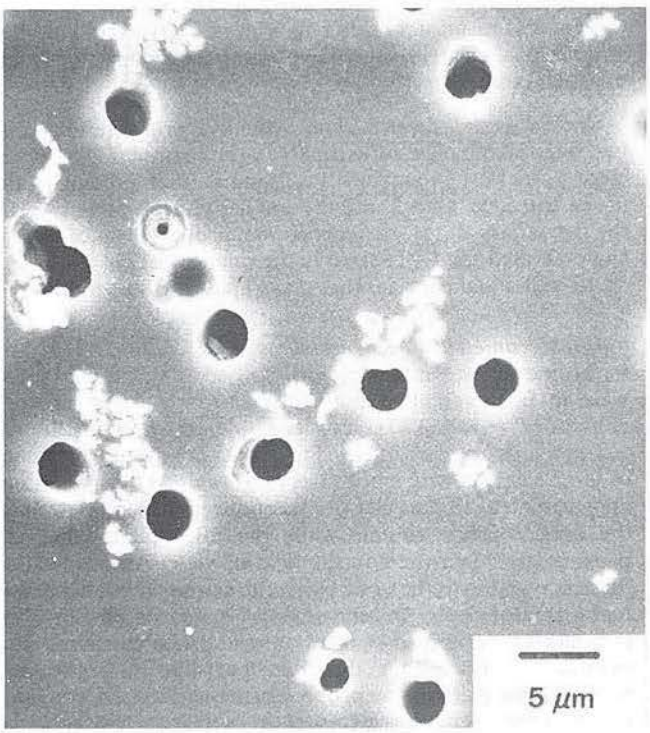

Primary filter – 5μm pore. 15.0 mps

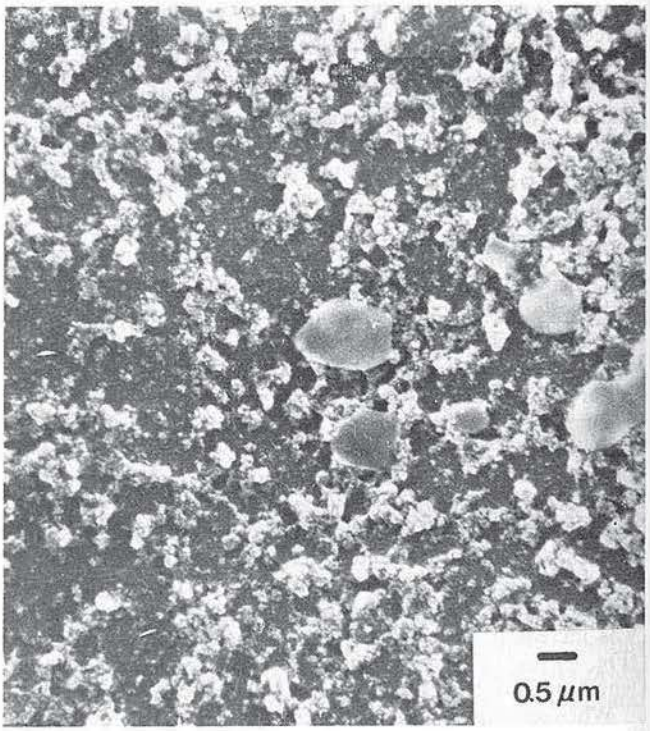

Secondary filter – 0.2μm pore. 15.0 mps

Fig. 6(*a*) Extractive probe conditions – effect of nitrogen dilution on particle morphology ($\phi = 0.2$) nominal nitrogen dilution flow

long chains of aggregated spheriods. Some of the chain structures become sufficiently long to deposit across a 5μm pore of the primary filter. This is then followed by a buildup of soot agglomerate within and finally over the clogged pore. As the resistance to flow through the pore increases, the deposition rate decreases and finally terminates, leaving a puff-like structure with a diameter close to the pore diameter (~5μm). Figure 7(*b*) provides supporting evidence since the puff-like structures are essentially monodispersed and few filter holes are visible.

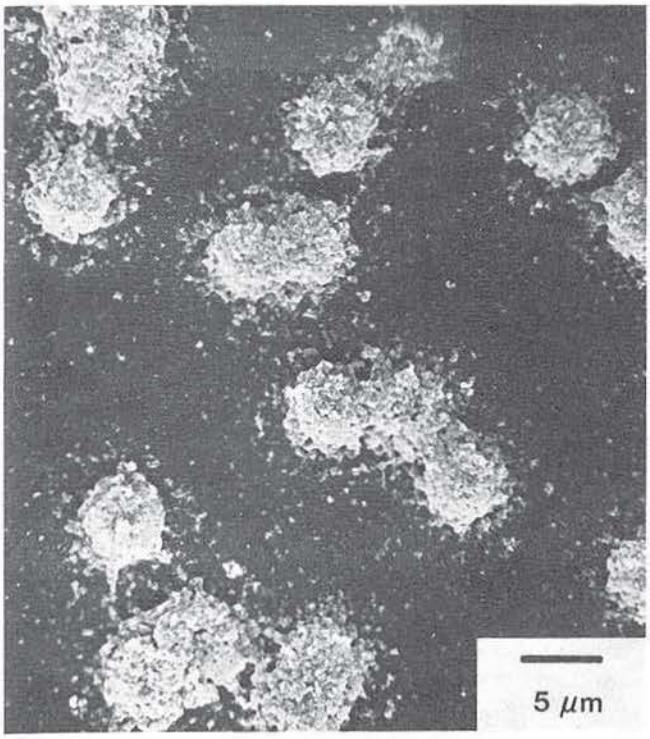

Primary Filter – 5μm pore. 0.65 mps

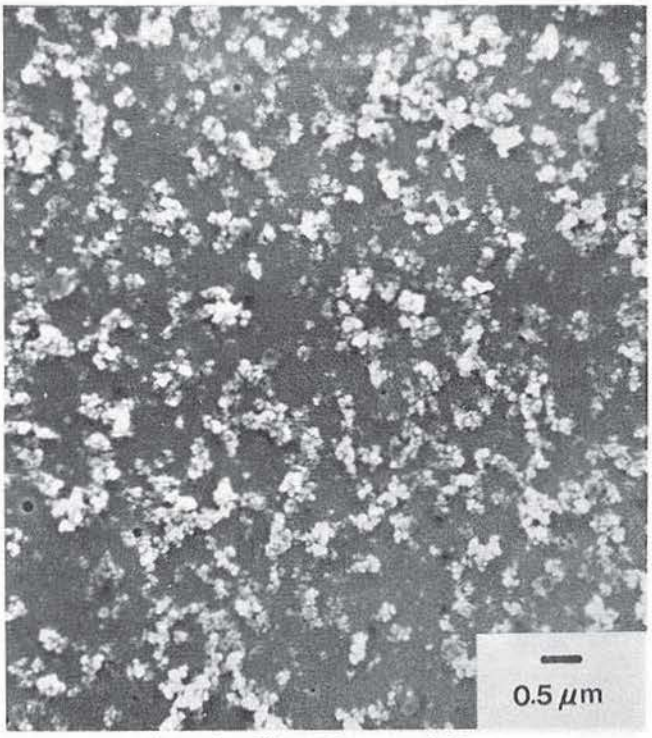

Secondary Filter – 0.2μm pore. 0.65 mps

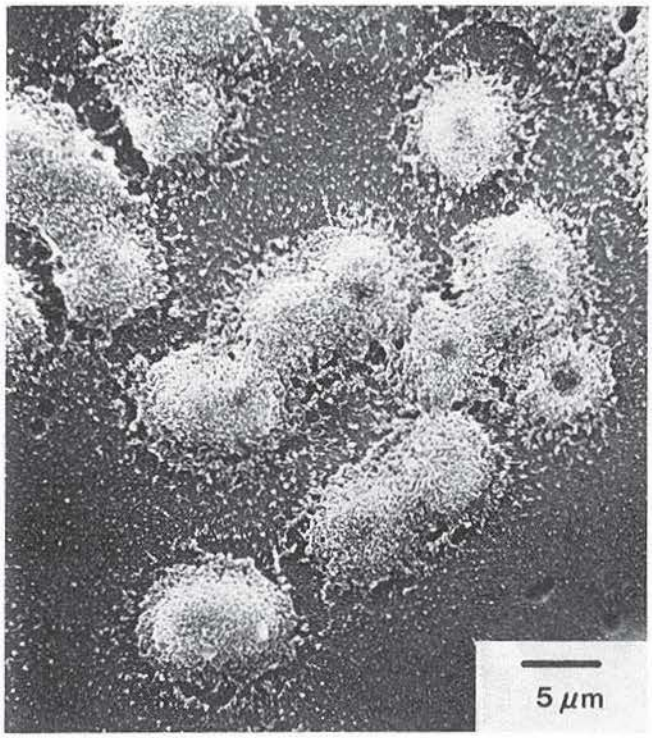

Primary Filter – 5μm pore. 15.0 mps

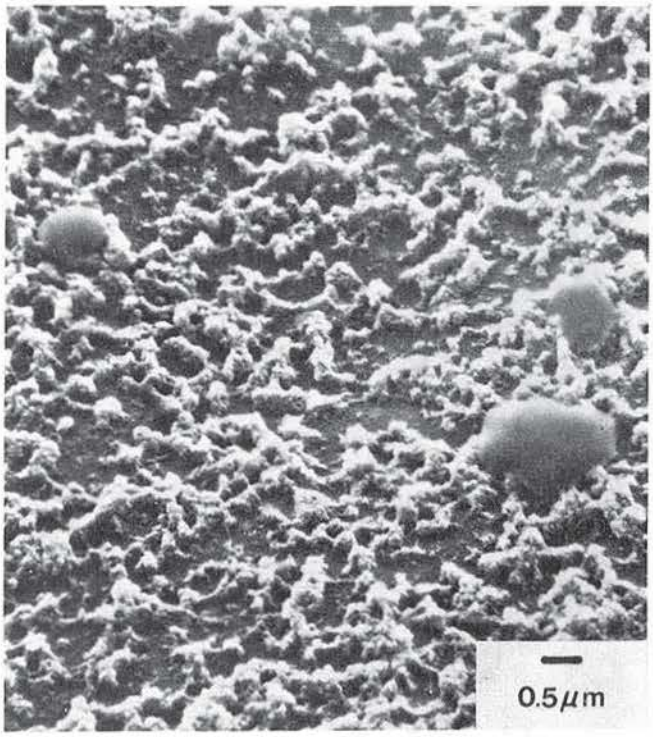

Secondary Filter – 0.2μm pore. 15.0 mps

Fig. 6(*b*) Extractive probe conditions – effect of nitrogen dilution of particle morphology ($\phi = 0.2$) zero nitrogen dilution flow

The $\sim 4\mu m$ particles detected optically at the probe entrance for the enriched ($\phi = 0.37$) condition were suspected of originating from a non-flame source. The measured size distribution (Fig. 9(*a*)) sported a peak size ($\sim 4\mu m$) whereas a monotonically increasing number density as size is reduced would have been anticipated. In the present case, the attrition of deposits off the centerbody was suspected. As a result, an evaluation was conducted during which the interferometric

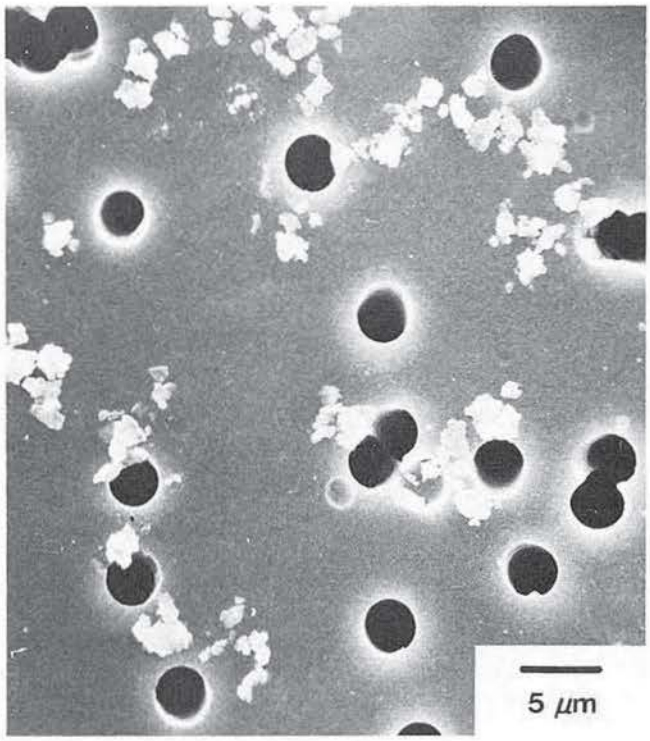

Primary filter-5μm pore

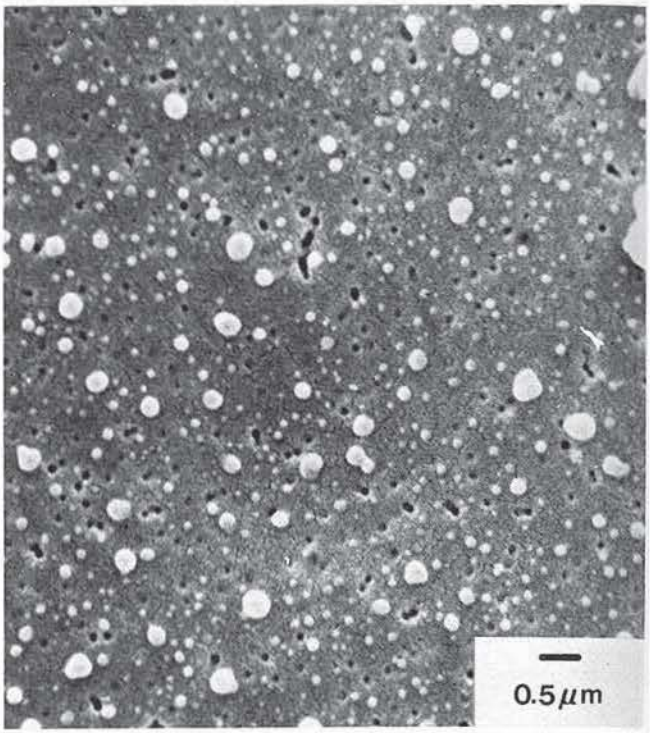

Secondary filter-0.2 μm pore

Fig. 7(a) $\phi = 0.2$

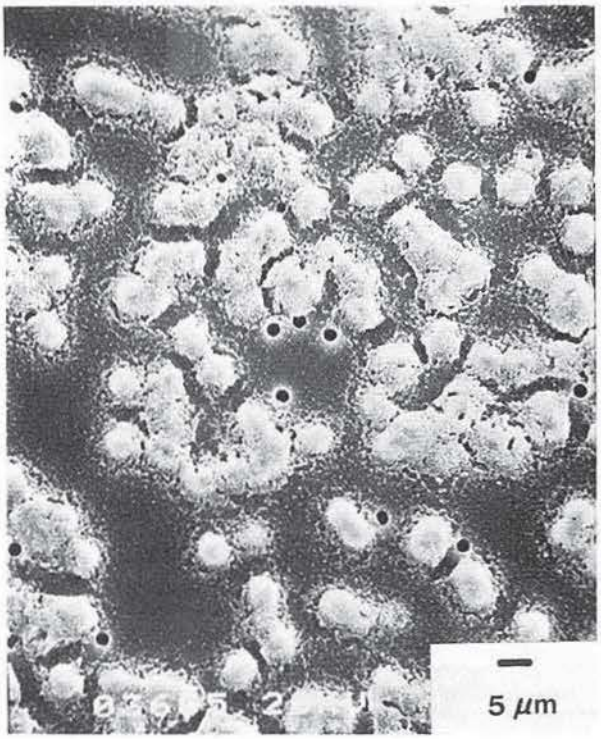

Secondary filter-0.2 μm pore

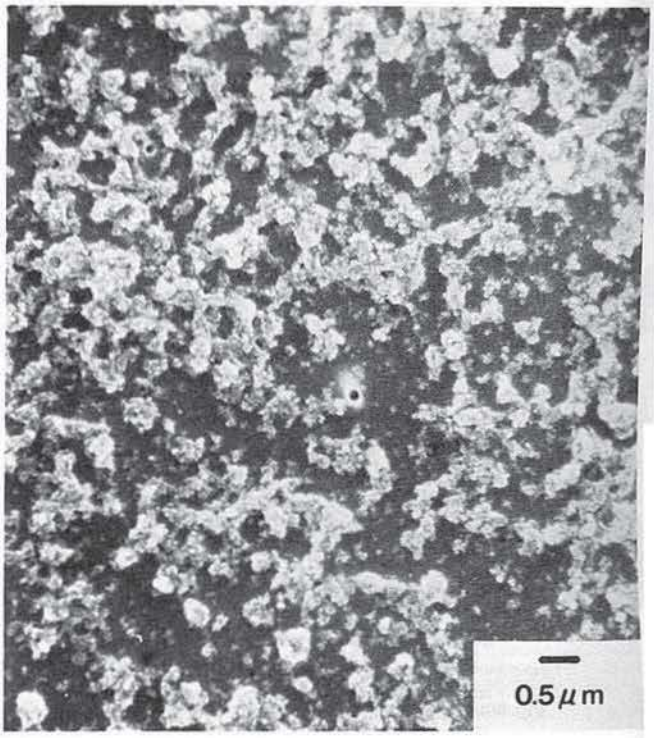

Primary filter-5μm pore

Fig. 7(b) $\phi = 0.37$

Fig. 7 Extractive probe conditions – effect of mixture ratio on number density (U_{ref} = 7.5mps, nominal nitrogen dilution flowrate)

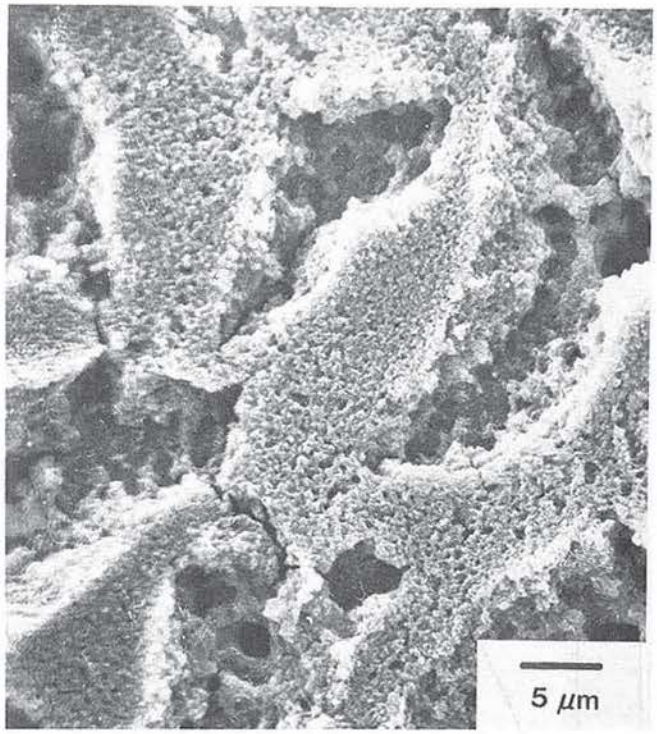

Fig. 8(a) Primary filter – 5μm pore

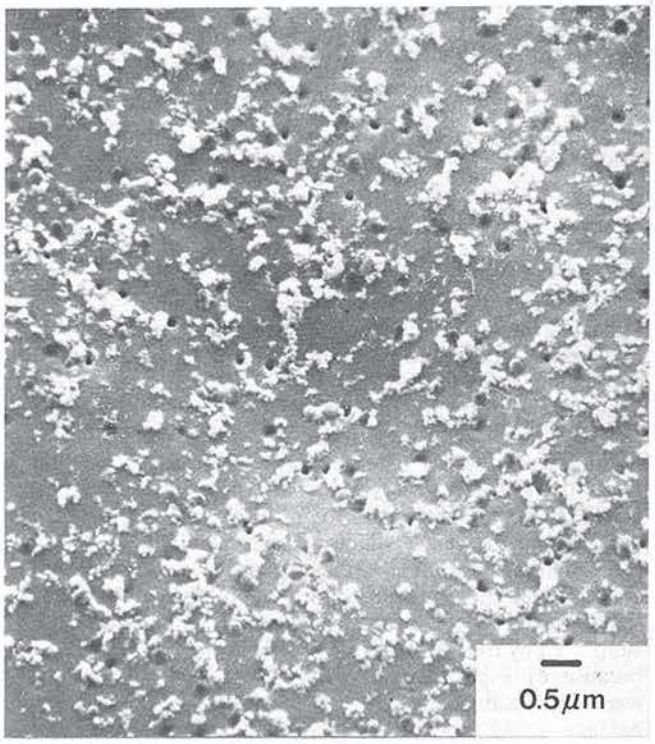

Fig. 8(b) Secondary filter – 0.2μm pore

Fig. 8 Extraction probe conditions – effect of water condensation on particle morphology (U_{ref} = 7.5mps, ϕ = 0.37, zero nitrogen flowrate)

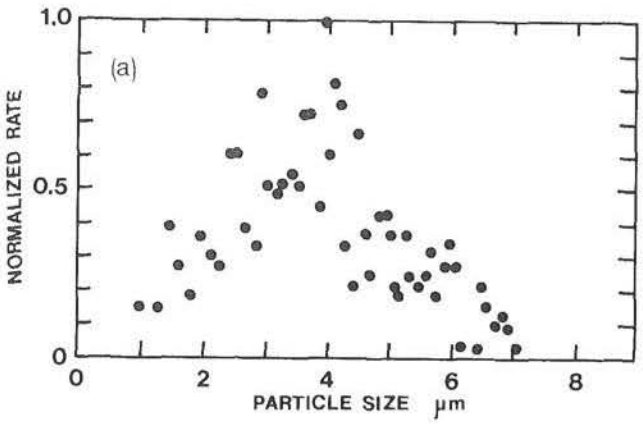

TOTAL RAW COUNT=631
TOTAL REDUCED COUNT(MM-2)=631
LINEAR MEAN=3.9
SURFACE MEAN=4.1
VOLUME MEAN=4.3
SAUTER MEAN=4.7
STANDARD DEV= 1.2

MEAN VELOCITY(M/S)=10.09
RMS VELOCITY(M/S)=2.43

Fig. 9(a) Interferometric Data

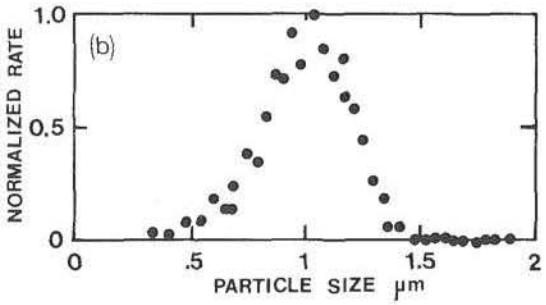

TOTAL RAW COUNT= 2585
TOTAL REDUCED COUNT= 169242.6
LINEAR MEAN = 1
SURFACE MEAN = 1.02
VOLUME MEAN = 1.04
SAUTER MEAN = 1.08
STANDARD DEV = .19

SAMPLE TIME= 22.2

Fig. 9(b) Ratioing Data

Fig. 9 Extractive probe conditions – representative optical probe sizing data (U_{ref} = 7.5mps, ϕ = 0.37)

data rate was monitored after the centerbody was cleaned. The rate increased in time as the centerbody was conditioned, and finally leveled off to a steady state (albeit low) reading. Although this evidence supports the suspicion, attrited particles from the centerbody have not yet been separately identified on the primary filter. One reason, of course, is the obscuration of attrited particles by the heavy loading of the puff-like structures at ϕ = 0.37.

The interferometric measurements also provide particle velocity. For example, at ϕ = 0.37 (Fig. 7(*b*) and 9), the average velocity of large particles (4μm peak) at the extractive probe entrance was 10.1mps (2.4mps S.D.). Calculation of the probe entrance velocity yielded an entrance velocity (uniform profile) of 15mps. These results suggest that the "isokinetic" setting in this swirling flow produced a flow rate close to but higher than desired.

Ratio Measurements (*~0.8 - 1.8μm*). Although the optical instrument was validated with 0.48μm particles for nonreacting conditions, in the enriched reacting flows (ϕ = 0.37) it was discovered that the presence of a large population of particles in the neighborhood of 1μm masked the observation of smaller particles. Thus, the theoretical dynamic

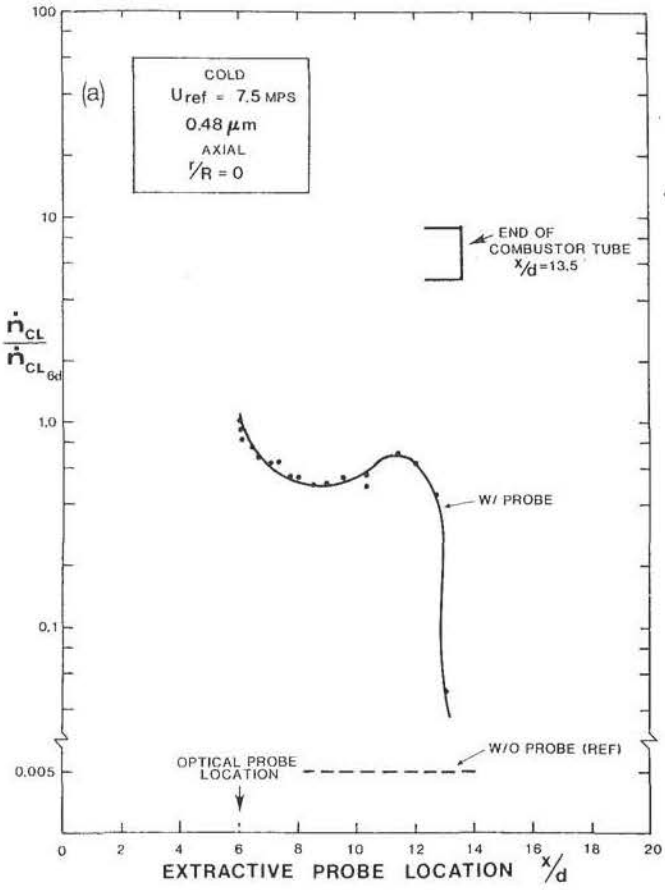

Fig. 10(a) Removal of extractive probe

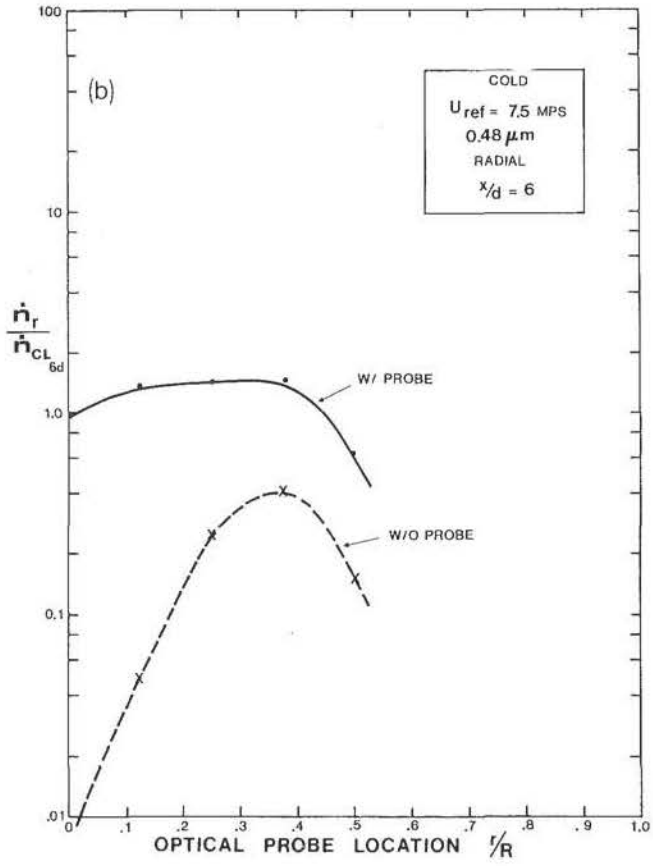

Fig. 10(b) Optical probe radial traverse

Fig. 10 Extractive probe perturbation – nonreacting flow with seeding (U_{ref} = 7.5mps, 0.48μm particles)

range of the ratioing technique (0.3 to 1.8μm) was limited in practice to ~0.8 to 1.8μm.

Despite this limitation, the ratioing measurements indicated that a substantial number of particles entering the extractive probe were of the "agglomerated" 1μm size. For example, ratioing data presented in Figure 9 in combination with the data rate recorded are entirely consistent with the size and number density observed on the SEM sample (Fig. 7(b)). The optically measured data rate increased as the mixture ratio was enriched, and as the sampling station was relocated from $6d$ to $3\frac{1}{2}d$. This result is again consistent with the SEM data. The effect of extractive probe condition on data rate is shown in Fig. 5. Data rates generally increase for these reacting flows with operating condition and sample volume location controlling the extent of change. Insight into these influences is presented in the extractive probe perturbation results that follow.

B. Extractive Probe Perturbation

1. Nonreacting Flow With Seeding. The extractive probe perturbation study was initiated by seeding a nonreacting flow with 0.48μm polystyrene particles, and recording the optically measured data rate as the extractive probe was removed axially from the optical probe volume.

In the present case, the study was conducted at 7.5mps and at an axial sampling station of $x/d = 6$. As shown in Fig. 10(a), the sample rate decreased as the extractive probe was withdrawn, with an overall decrease of more than 200-fold between the with-extractive-probe ("w/probe") and without-extractive-probe ("w/o probe") conditions. The relatively low sample rate in the absence of the extractive probe is due to the strong, swirl-induced centrifugal force on the particles. When the probe is present, this force is reduced and particles can more freely diffuse radially toward the centerline. The radial diffusion of the particles becomes evident by examining Fig. 10(b). Two observations are noteworthy from this figure. First, the without-probe profile exhibits a very small data rate in the center which increases radially. This shows that diffusion is quite small and that very few particles are able to reach the central core of the combustor. However, in the presence of the probe, diffusion is enhanced. This is supported by the flat data rate profile in the figure. Secondly, because of experimental difficulties, radial measurements were not obtained beyond $r/R = 0.5$, thus a particle rate balance could not be performed based on these radial measurements.

2. Reacting Flow. The presence of the extractive probe produced an impact on the optically measured data rate that ranged from a small to a substantial effect depending on the operating conditions. For example, at 5.5mps, $\phi = 0.37$, and at the sampling station $x/d = 6$, the data rate remained relatively constant (Fig. 11) as the extractive probe was separated from the optical probe. In addition, no observable change in the optically measured particle size was recorded. The radial profiles also remain similar for both the with-

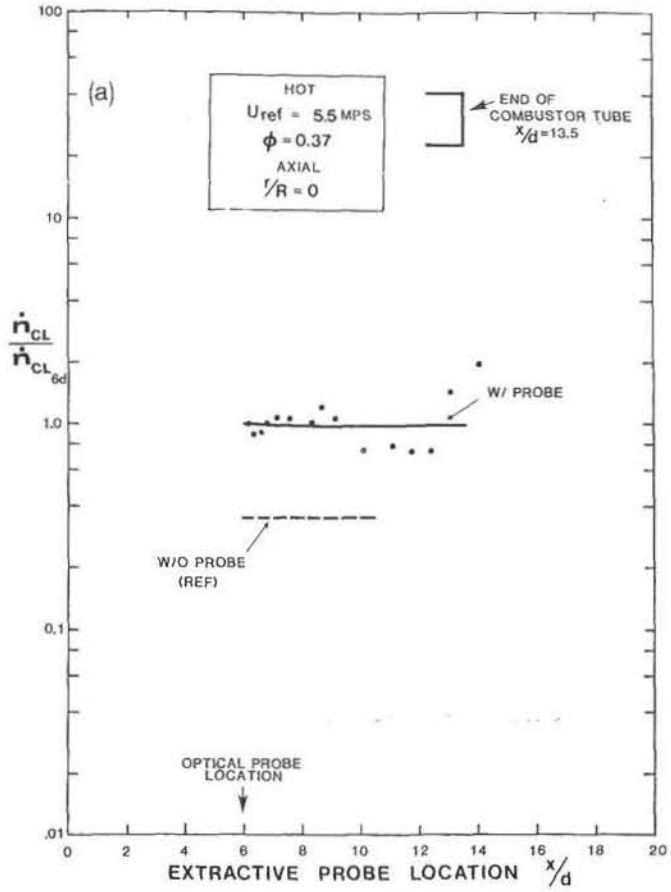

Fig. 11(a) Removal of extractive probe

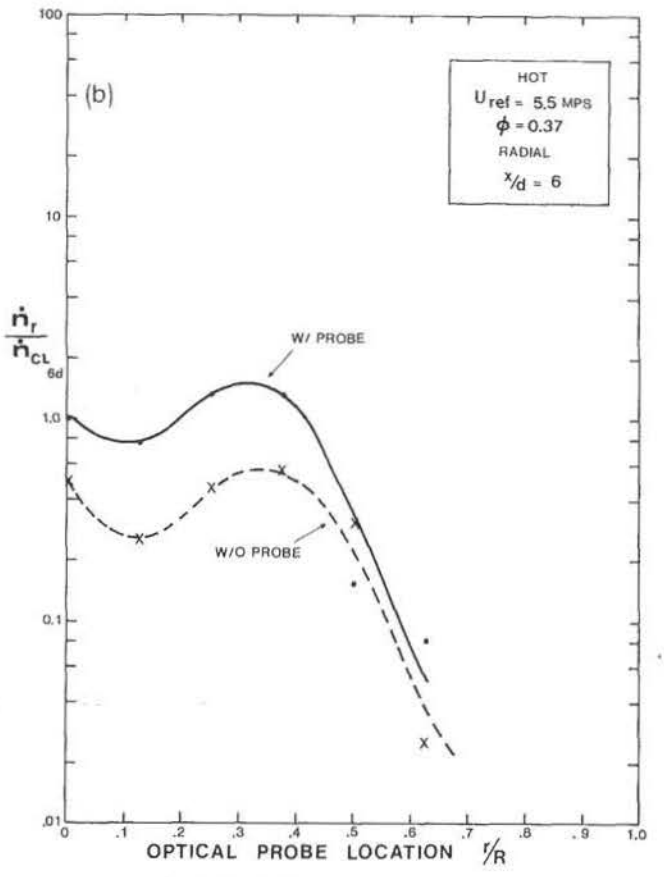

Fig. 11(b) Optical probe radial traverse

Fig. 11 Extractive probe perturbation – reacting flow (U_{ref} = 5.5mps, ϕ = 0.37)

probe and without-probe condition.[1] The lack of change in these measurements is probably due to a relatively small axial and radial gradients in flow properties at this sampling location as a result of the upstream recirculation and mixing.

Closer to the centerbody (x/d = 3½), the results are dramatically different (Fig. 12(*a*)). Here, the sampling station is located within the recirculation zone (refer to Fig. 1). The sample rate increased more than 70-fold as the probe was withdrawn from the optical sampling volume, with the steepest gradient in data rate occuring within 2 centerbody diameters of the sampling station. The change then is likely a result of a substantial perturbation of the local flow field with a concomitant change in mixing, chemistry, and temperature due to the intrusion of a solid, cold body into a zone of reverse flow. It is noteworthy that the effect on data rate levels off at approximately 6 centerbody diameters downstream of the recirculation zone, and the data rate settles to the without-probe condition.

The substantial probe perturbation is further evidenced in the radial profiles (Fig. 12(*b*)). Here, the with-probe profile resembles the previous case (Fig. 11(*b*)). However, the without-probe profile is markedly different, having a distinct maximum data rate on the centerline and decreasing monotonically radially outward.

Increasing the reference velocity from 5.5 to 7.5mps produced an even more dramatic impact even though the sampling volume was located in the wake of the recirculation zone (x/d = 6). Again, the sample rate increased about 40-fold as the probe was removed from the sampling volume (Fig. 13(*a*)). However, for this case there is an appreciable scatter in the measurements. This is attributed to a small but perceptible change in the flame structure, probably due to blockage, as the extractive probe was moved from one location to another. In particular, the flame compressed, and the wake region moved upstream as the extractive probe was moved toward the centerbody. The extractive probe perturbation was therefore not limited just to *local* changes (as in the previous two cases), but extended to dominate flame behavior throughout the combustor. This gross impact on data rate notwithstanding, the change in particle size in the range measured optically was not appreciable. The radial profiles (Fig. 13(*b*)) resemble the last case (5.5mps, ϕ = 0.37, x/d = 3½), showing both the large increase in data rate and large change in the presence of the probe.

The effect of extractive probe sample flowrate on the data rate observed optically at the probe entrance was earlier shown (Fig. 5) to be influenced by combustor operating condition and sample volume location. The extractive probe perturbation results provide some explanation of these trends. At 5.5mps, ϕ = 0.37, and x/d = 6, the perturbation of the extractive probe is minimal and the effect of an increase in sample flowrate is to increase the data rate to the same degree observed in the nonreacting flow tests. At 3½d, the sampling volume is in the recirculation zone. An increase in sample flowrate has no effect on data rate, which indicates that the

[1] The factor of two difference (Fig. 11(*b*)) in data rate at r/R = 0 is not significant and within the reproducibility at ϕ = 0.37. For example, a two-fold change in data rate was observed for small changes (e.g., $\Delta\phi$ = 0.01) in mixture ratio.

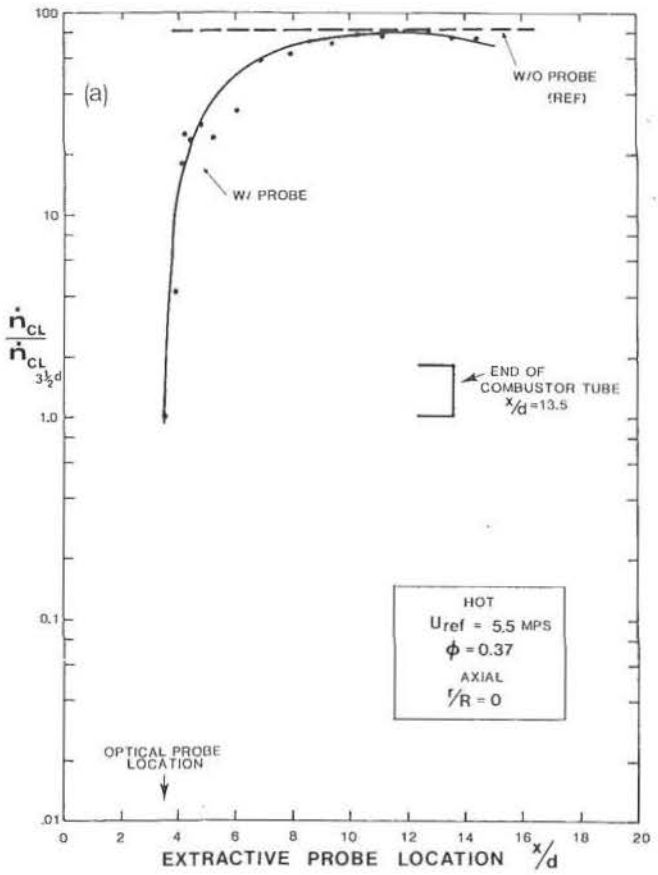

Fig. 12(a) Removal of extractive probe

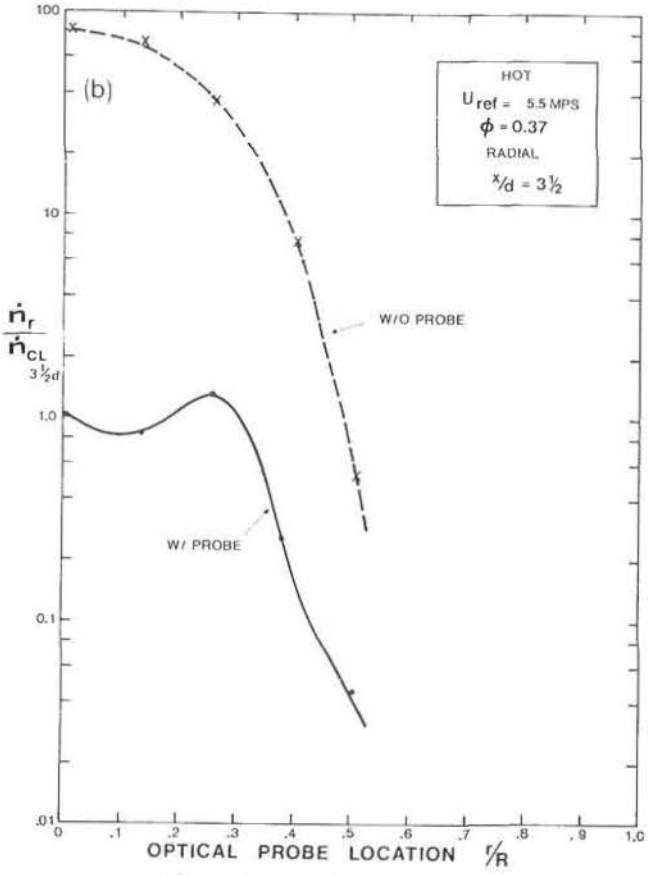

Fig. 12(b) Optical probe radial traverse

Fig. 12 Extractive probe perturbation – reacting flow (U_{ref} = 5.5mps, ϕ = 0.37)

flow aerodynamics fully control the local flow properties. Finally, at 7.5mps, $\phi = 0.37$, and $x/d = 6$, the blockage of the probe dominates and, because the blockage is influenced by sample flowrate, an increase in flowrate was observed to produce a perceptible change in flame structure and, as a result, a substantial change in data rate.

Summary

The present study represents an exploratory investigation into the sample integrity and perturbation associated with extractive probe sampling for soot. The use of nonintrusive optical measurement techniques focused at the entrance of an extractive probe provided a unique and independent measurement of number density (i.e., data rate) and particle size in the range of 0.3μm to 7.5μm for nonreacting flow and ~0.8μm to 7.5μm in the case of reacting flow.

The results pertaining to extractive probe sampling conditions provided new insights as well as reinforcing the traditionally perceived "isokinetic" effect. For example, number density increased with an increase in sample flowrate. However, the entrance velocity calculated from the isokinetically set sample flowrate in this swirl-stabilized flow was found to be 50 percent above the optically measured velocity. In addition, the optical measurements allowed the identification of a non-flame source of particulate – in this case, the attrition of particles off the centerbody.

Changes in nitrogen cooling rate did not affect the optical measurement, but did affect the morphology and number density on the 5μm filter. Higher sample temperatures and lower cooling rates produced a larger chain soot structure that subsequently clogged and built up in the 5μm pores giving the illusion of a monodisperse distribution. For high cooling rates, platelet-like structures were formed, likely as a product of rapidly condensing heavily concentrated fuel pockets extracted in an early stage of pyrolysis.

The effect of the physical presence of the extractive probe varied from no significant impact on data rate and particle size (in the particle size range measured) to a dramatic effect on data rate. The dramatic perturbation occurred when the sampling volume was located in the recirculation zone, or when the reference velocity was increased beyond the value (5.5mps in the present case) above which the blockage produced by the extractive probe becomes significant.

The results reported here are undoubtedly specific to the combustor configuration employed, and the size and design of the extractive probe used. In addition, the results are limited by the small particle size cutoff for the optical technique. As a result, the effect of extractive probe conditions and perturbation on soot particle formation, and on formed soot particles in the size range considered to be heavily populated ($\sim .02\mu m \leq dp \leq 0.3\mu m$) requires an expanded optical capability. This notwithstanding, the present results reveal:

- The type of problems associated with extractive probes
- Questions that must be raised in the interpretation of data from extractive and optical probes
- The type of experiments necessary to develop and test

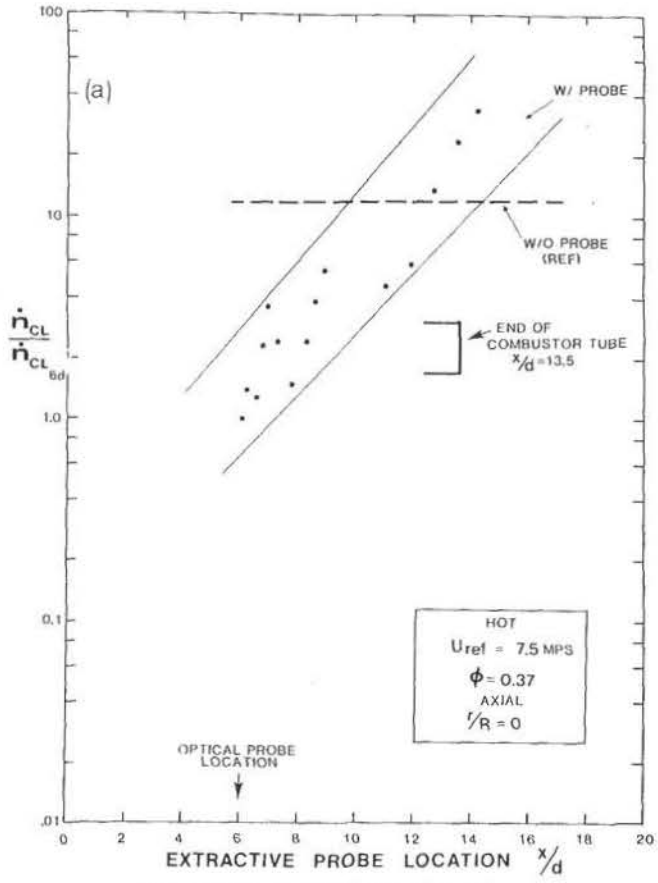

Fig. 13(a) Removal of extractive probe

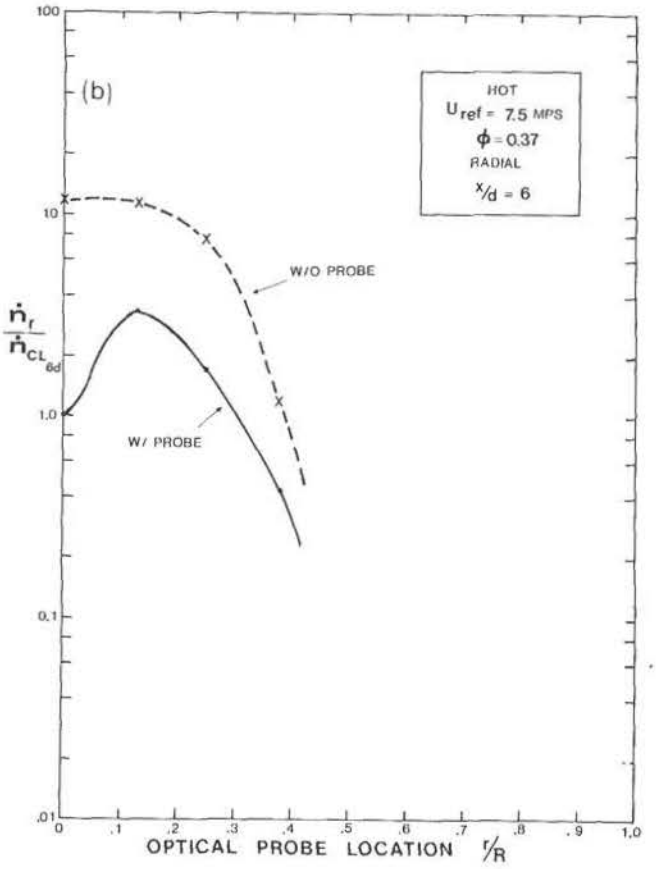

Fig. 13(b) Optical probe radial traverse

Fig. 13 Extractive probe perturbation – reacting flow ($U_{ref} = 7.5, \phi = 0.37$)

methods employed to measure soot in gas turbine applications.

Acknowledgment

The results presented were obtained in a soot formation/alternative fuels study in progress at the UCI Combustion Laboratory and supported by the Air Force Engineering and Service Center, Research and Development Directorate, Environics Division (Air Force Contract #FO-8635-79-C-0158) with Captain Harvey Clewell as the project monitor.

References

1 Glassman, I., and Yaccarino, P., "The Temperature Effect in Sooting Diffusion Flames," Eighteenth Symposium (International) on Combustion, The Combustion Institute, 1981.

2 Blazowski, W. S., "Dependence of Soot Production on Fuel Blend Characteristics and Combustion Conditions," ASME Paper 79-GT-155, presented at ASME Gas Turbine Conference, San Diego, Mar. 1979.

3 Schirmer, R. M., "Effect of Fuel Composition on Particulate Emission from Gas Turbine Engines," in *Emissions from Continuous Combustion Systems*, Plenum Press, New York, 1972, p. 189.

4 Clark, V. A., Leonard, J. A., and Mellor, A. M., "Soot Loadings, Radiation Intensities, Gaseous Species Concentrations and Temperatures in a Quasi-Steady Spray Flame," in *Particulate Carbon Formation During Combustion*, Plenum Press, New York, 1981.

5 Hirleman, E. D., "Optical Technique for Particulate Characterization in Combustion Environments: The Multiple Ratio Single Particle Counter," Ph.D. thesis, Purdue University, Aug. 1977.

6 Bachalo, W. D., Hess, C. F., and Hartwell, C. A., "An Instrument for Spray Droplet Size and Velocity Instruments," ASME *Journal of Engineering for Power*, Vol. 102, No. 4, Oct. 1980, p. 798.

7 Hodkinson, J. R., "Light Scattering and Extinction by Irregular Particles Larger than the Wavelength," *Proceedings of Interdisciplinary Conference on Electromagnetic Scattering*, Permagon Press, Oxford, 1963, p. 87.

8 Chu, W. P., and Robinson, D. M., "Scattering from a Moving Spherical Particle by Two Crossed Coherent Plane Waves," *Applied Optics*, Mar. 1977, p. 619.

9 Moses, C. A., and Naegeli, D. W., "Fuel Property Effects on Flame Radiation in Aircraft Turbine Combustors," WSS/CI Paper 80-9, presented at the 1980 Spring Meeting, Western States Section/Combustion Institute, Irvine, Apr. 1980.

10 Sawyer, R. F., "Experimental Studies of Chemical Processes in a Model Gas Turbine Combustor," in *Emissions from Continuous Combustion Systems*, Plenum Press, New York, 1972, p. 243.

11 Fenton, D. L., Luebcke, E. H., and Norstrom, E., "Physical Characterization of Particulate Material from a Turbine Engine," ASME Paper 79-GT-179, presented at the ASME Gas Turbine Conference, San Diego, Mar. 1979.